Context-dependent operation of neural circuits underlies a navigation behavior in *Caenorhabditis elegans*

Muneki Ikeda[a], Shunji Nakano[a,b], Andrew C. Giles[a,c], Linghuan Xu[a], Wagner Steuer Costa[d,e], Alexander Gottschalk[d,e], and Ikue Mori[a,b,1]

[a]Group of Molecular Neurobiology, Division of Biological Science, Graduate School of Science, Nagoya University, 464-8602 Nagoya, Japan; [b]Neuroscience Institute, Graduate School of Science, Nagoya University, 464-8602 Nagoya, Japan; [c]Department of Neuroscience, The Scripps Research Institute, Scripps Florida, Jupiter, FL 33458; [d]Buchmann Institute for Molecular Life Sciences, Goethe University, 60438 Frankfurt, Germany; and [e]Department of Biochemistry, Chemistry and Pharmacy, Institute for Biophysical Chemistry, Goethe University, 60438 Frankfurt, Germany

Edited by Paul W. Sternberg, California Institute of Technology, Pasadena, CA, and approved February 3, 2020 (received for review October 28, 2019)

The nervous system evaluates environmental cues and adjusts motor output to ensure navigation toward a preferred environment. The nematode *Caenorhabditis elegans* navigates in the thermal environment and migrates toward its cultivation temperature by moving up or down thermal gradients depending not only on absolute temperature but on relative difference between current and previously experienced cultivation temperature. Although previous studies showed that such thermal context-dependent opposing migration is mediated by bias in frequency and direction of reorientation behavior, the complete neural pathways—from sensory to motor neurons—and their circuit logics underlying the opposing behavioral bias remain elusive. By conducting comprehensive cell ablation, high-resolution behavioral analyses, and computational modeling, we identified multiple neural pathways regulating behavioral components important for thermotaxis, and demonstrate that distinct sets of neurons are required for opposing bias of even single behavioral components. Furthermore, our imaging analyses show that the context-dependent operation is evident in sensory neurons, very early in the neural pathway, and manifested by bidirectional responses of a first-layer interneuron AIB under different thermal contexts. Our results suggest that the contextual differences are encoded among sensory neurons and a first-layer interneuron, processed among different downstream neurons, and lead to the flexible execution of context-dependent behavior.

neural circuits | context dependency | *C. elegans* | navigation behavior | behavioral modeling

The nervous system detects environmental cues and adjusts motor commands for navigation toward preferred environments (1, 2). What constitutes a preference depends on situation and context, thus animals need to integrate environmental stimuli with contextual information for appropriate motor responses. Such context-dependent neural processing is critical for the flexible migration of animals (3, 4). However, the neural circuit basis of context-dependent behavioral regulation is not well understood.

Despite having a compact nervous system consisting of only 302 neurons, the nematode *Caenorhabditis elegans* can navigate thermal gradients, known as thermotaxis. Importantly, their navigation drastically changes depending on thermal context: their position on the thermal gradient relative to a temperature they recently experienced and memorized because they found food in that condition (5–8). For experimentation, we define this thermal context as the difference between their current temperature on the gradient (T) and their cultivation temperature (T_c), set by cultivating animals with food at a certain temperature. On a thermal gradient without food, animals migrate up the thermal gradient toward T_c when T is 1 to 5 °C lower than T_c ($T < T_c$) and migrate down the gradient when T is 1 to 5 °C higher than T_c ($T > T_c$) (Fig. 1 *A*–*C*). When T is much higher than T_c ($T >> T_c$), animals still manage to migrate toward T_c, whereas when T is much lower than T_c ($T << T_c$), animals hardly migrate toward T_c (Fig. 1 *B* and *C*). In the region where T is close to T_c ($T \sim T_c$), animals perform isothermal tracking behavior (6, 9) (Fig. 1 *B* and *D*).

Previous studies have dissected thermotaxis by analyzing reorientation behavior, a typical behavioral component of *C. elegans* (10). During migrations toward T_c, the exit direction after reorientation is biased in a thermal context-dependent manner; in the $T < T_c$ condition, the animals exit turns more frequently toward higher temperature, while they exit turns more frequently toward lower temperature in the $T > T_c$ condition (11). Also, the frequency of reorientation is biased to drive animals toward T_c when T is higher than T_c ($T > T_c$ and $T >> T_c$) (11, 12). However, there has been no study showing what kinds of neural pathways are responsible for thermal context-dependent behavioral regulation. More importantly, although the major thermosensory neurons AFD, AWC, and ASI are known to show different responsive ranges to thermal stimuli (13–16), it remains entirely elusive how context is encoded and evaluated by the nervous system.

By conducting high-resolution behavioral analysis, comprehensive cell ablation, and computer modeling, we show here that opposing biases of even single behavioral components are generated

Significance

A free-living nematode *Caenorhabditis elegans* memorizes an environmental temperature and migrates toward the remembered temperature on a thermal gradient by switching movement up or down the gradient. How does the *C. elegans* brain, consisting of 302 neurons, achieve this memory-dependent thermotaxis behavior? Here, we addressed this question through large-scale single-cell ablation, high-resolution behavioral analysis, and computational modeling. We found that depending on whether the environmental temperature is below or above the remembered temperature, distinct sets of neurons are responsible to generate opposing motor biases, thereby switching the movement up or down the thermal gradient. Our study indicates that such a context-dependent operation in neural circuits is essential for flexible execution of animal behavior.

Author contributions: M.I., S.N., and I.M. designed research; M.I. and L.X. performed research; M.I., S.N., A.C.G., L.X., W.S.C., A.G., and I.M. contributed new reagents/analytic tools; M.I. and L.X. analyzed data; and M.I., S.N., A.C.G., A.G., and I.M. wrote the paper.

The authors declare no competing interest.

This article is a PNAS Direct Submission.

Data Deposition: Source code is available at GitHub, https://github.com/ikedamuneki/ThermotaxisAnalysis.

[1]To whom correspondence may be addressed. Email: m46920a@nucc.cc.nagoya-u.ac.jp.

This article contains supporting information online at https://www.pnas.org/lookup/suppl/doi:10.1073/pnas.1918528117/-/DCSupplemental.

First published March 2, 2020.

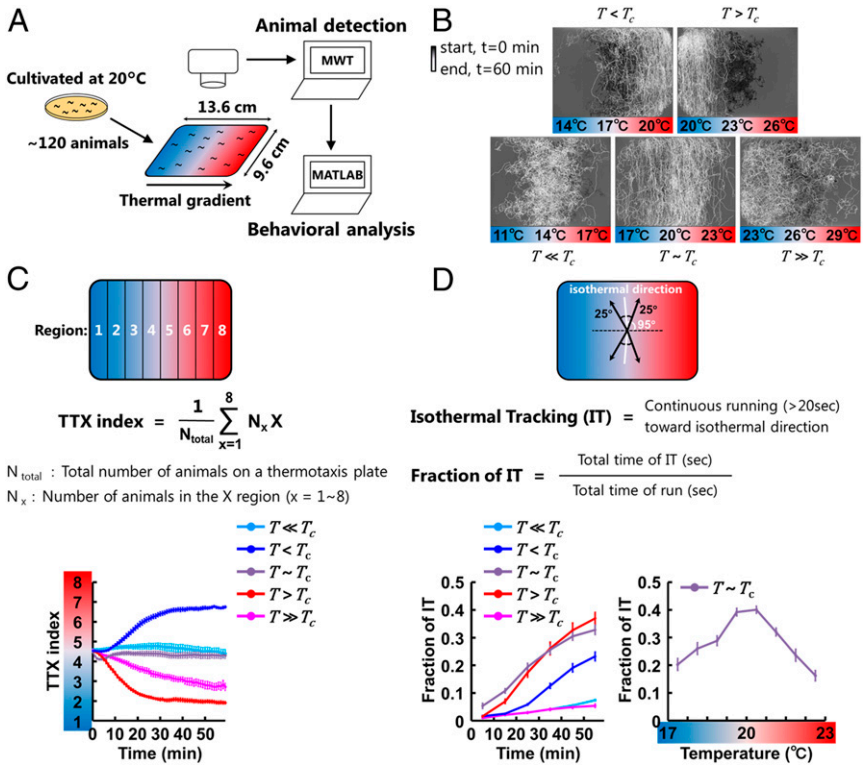

Fig. 1. Thermotaxis behavior changes in thermal environments (T) relative to the cultivation temperature (T_c). (*A*) MWT system for the extraction of behavioral components during thermotaxis behavior. The thermotaxis assays were performed as previously reported (5). The positions and postures of animals were captured by the MWT system and then analyzed by custom-built MATLAB scripts. (*B*) Animals cultivated at 20 °C were placed on a TTX plate with a thermal gradient with 14 °C (*Lower Left*, $T << T_c$), 17 °C (*Upper Left*, $T < T_c$), 20 °C (*Lower Middle*, $T \sim T_c$), 23 °C (*Upper Right*, $T > T_c$), or 26 °C (*Lower Right*, $T >> T_c$) at the center. Shown here are the representative trajectories of ~120 animals that were recorded by MWT. The time from the start of the assays is represented in gray scale. (*C*) The time course of TTX indices calculated using the described equation and averaged within the assays ($n = 7$ to 12). Error bars indicate SEM. (*D*) IT is defined as continuous moving toward isothermal direction ±25° for longer than 20 s (*Upper*). Isothermal direction was tilted by 5° along the distortion of the thermal gradients near the edges of the plates. *Lower Left* shows the time course of fractions of IT. *Lower Right* shows the fraction of IT as a function of the absolute temperature during 30 to 60 min after the start of the assays. In *C* and *D*, cyan lines correspond to experiments in the $T << T_c$ condition, blue lines correspond to experiments in the $T < T_c$ condition, purple lines correspond to experiments in the $T \sim T_c$ condition, red lines correspond to experiments in the $T > T_c$ condition, and magenta lines correspond to experiments in the $T >> T_c$ condition.

by distinct sets of neurons under different thermal contexts. We identify multiple neural pathways that regulate behavioral components of *C. elegans* locomotion during thermotaxis, such as turns, reversals, curves, and speed, each of which contributes to thermotaxis to different degrees depending on thermal context. Calcium-imaging analyses in freely moving animals suggest that the thermosensory neurons AFD and AWC implement the context-dependent encoding of thermal signals. Intriguingly, thermal signals are likely to be oppositely processed in a first-layer interneuron AIB, depending on whether T is lower or higher than T_c ($T < T_c$ or $T > T_c$). Also, in immobilized animals, AIB oppositely responds to thermal signals: temperature increments inhibit the activity of AIB in $T < T_c$ but enhance the activity in $T > T_c$. Our results suggest that different thermal contexts are evaluated in sensory neurons and evoke bidirectional responses in the AIB first-layer interneuron, thereby resulting in context-dependent behavioral regulation.

Results

How Thermotaxis Is Executed Depends on the Relative Position to the Cultivation Temperature. We assessed *C. elegans* thermotaxis by employing a Multi-Worm Tracker (MWT) (17). The MWT simultaneously captured the positions and postures of ~120 animals (Fig. 1*A*). To conduct thermotaxis assays, we set the cultivation temperature (T_c) as 20 °C. Animals were placed at the center of an assay plate, which itself was centered at 14 °C, 17 °C, 20 °C, 23 °C, or 26 °C, thus testing five different contexts $T << T_c$, $T < T_c$, $T \sim T_c$, $T > T_c$, and $T >> T_c$, respectively (Fig. 1*B*). The animals' migrations were evaluated by calculating a thermotaxis index (TTX index), according to the equation shown in Fig. 1*C*. The TTX index is 1 when all of the animals are in the coldest fraction of the plate and 8 when all of the animals are in the warmest fraction. Consistent with our previous report (5, 7), the animals reached their T_c within ~30 min in the $T < T_c$ and $T > T_c$ conditions (Fig. 1*C*, Movie S1, and Dataset S1), whereas the animals moved toward the T_c more slowly in the $T >> T_c$ condition. In the $T << T_c$ condition, animals did not move to the T_c.

The data extracted through the MWT were further analyzed by a custom-built MATLAB script (Fig. 1*A*) (18), in which isothermal tracking (IT) is defined as continuous movement perpendicular to the gradient (±25°) for longer than 20 s, thereby staying at the same temperature (Fig. 1*B*). In $T < T_c$, $T \sim T_c$, and $T > T_c$ conditions, the fractions of IT behavior increased during the assays more dramatically than the other conditions (Fig. 1*D*). The fraction was highest at the region close to the T_c, as previously reported (9, 19).

In summary, the animals moved up the thermal gradient in the $T < T_c$ condition, down the gradient in the $T > T_c$ condition, gradually moved down in the $T >> T_c$ condition, did not move up in the $T << T_c$ condition, and executed IT in the region near the T_c.

Ablation and Silencing of Single Neurons Show Distinct Impact on Thermotaxis in Different Thermal Contexts. To identify sets of neurons required for thermotaxis in the different contexts, we

conducted assays using cell-ablated/silenced animals. We chose 17 classes of neurons as our targets of investigation for their roles in thermotaxis (Fig. 2*A*). These include three classes of thermosensory neurons (AFD, AWC, and ASI) (9, 13–15), two classes of locomotory command interneurons that had been shown to regulate backward locomotion (AVA and AVE) (20, 21), four classes of head motor neurons that had been shown to regulate steering behavior (RMD, RME, SMB, and SMD) (22–24), and eight classes of interneurons that are predicted to be critical for mediating transmission or integration of information (AIA, AIB, AIY, AIZ, RIA, RIB, RIM, and RIS) (25–28). For each of these neurons, we conducted single-cell ablation by two methods: expressing reconstituted caspases (29) or expressing and photoactivating mito-miniSOG ("miniature Singlet Oxygen Generator," a protein producing toxic oxygen radicals in response to blue light) (30) (*SI Appendix*, Table S1 and *Materials and Methods*). We also acutely silenced the neurons individually by expressing HisCl1 (a histamine-gated chloride channel) and exposing animals to histamine (31) (*SI Appendix*, Table S2 and *Materials and Methods*).

First, we investigated how individual cell ablation and silencing affect the IT behavior by measuring the fraction of IT 30 to 60 min after the start of the assays. Consistent with our previous report (9), the single ablation/silencing of AFD, AIY, and RIA diminished the fraction of IT following all three types of genetic manipulations (Fig. 2*B*, *SI Appendix*, Fig. S1*A*, and Dataset S2). We also found that the single ablation/silencing of SMB, SMD, and RMD equally strongly impaired the fraction of IT, indicating that these head motor neurons are required for the IT behavior.

We then evaluated the impact of ablation/silencing of individual cells on the migration of animals toward the T_c by comparing TTX indices at the end of the assays. In the $T >> T_c$ condition, the single ablation/silencing of AWC, RIB, AVA, RMD, and SMD significantly impaired the decrement of TTX indices following all three types of genetic manipulations (Fig. 2*C*, *SI Appendix*, Fig. S1*B*, and Dataset S2), although these neurons we identified do not form a continuous pathway from sensory to motor layers. In the $T < T_c$ condition, the single ablation/silencing of only AFD and AIB significantly impaired the increment of TTX indices following all three types of genetic manipulations, whereas in the $T > T_c$ condition, we hardly identified the neurons that consistently impaired the decrement of TTX indices (Fig. 2*D*, *SI Appendix*, Fig. S1*B*, and Dataset S2).

Through cell ablation/silencing analyses, we identified neurons required for the IT behavior in the $T \sim T_c$ condition (Fig. 2*B*). However, we did not clarify a comprehensive neural pathway for thermotaxis in the $T < T_c$, $T > T_c$, or $T >> T_c$ condition, suggesting that more detailed behavioral analysis is necessary to identify sets of neurons responsible for the context-dependent thermotaxis migration.

Thermal Context-Dependent Regulation of Behavioral Components Ensures Migrations toward the Cultivation Temperature. *C. elegans* is known to navigate using a series of stereotyped movements, designated behavioral components (10, 32, 33). We thus detected the behavioral components from the data extracted through the MWT by using a custom-built MATLAB script (Fig. 1*A* and *SI Appendix*, *Materials and Methods*). Behavior was first divided into three behavioral classes: turns, reversals, and curves (Fig. 3*A*). Turns were further classified into omega turns and shallow turns (34, 35), and reversals were further classified into reversals and reversal turns (10, 33, 36). To understand how each of the behavioral components are regulated during the migrations toward T_c, we focused on the first 30 min from the start of the assays and analyzed the animals that were distributed in the center four fractions of the assay plate; 15.5 to 18.5 °C for the $T < T_c$ condition and 21.5 to 24.5 °C for the $T > T_c$ condition (Fig. 3*B*).

Our analyses showed that turns and reversals were oppositely biased depending on whether the animals were moving below or above the T_c ($T < T_c$ or $T > T_c$ conditions, respectively) (Fig. 3 *C* and *D* and Dataset S1). The frequencies of turns and reversals were measured as a function of the entry directions θ, where θ is the angle between the moving direction right before these behavioral events and the vector pointing to the warm side of the thermal gradient (Fig. 3*C*). In the $T < T_c$ condition, the frequencies of turns and reversals were higher when the animals were moving down the thermal gradient ($\theta > 90$) than when the animals were moving up the thermal gradient ($\theta < 90$), whereas in the $T > T_c$ condition, the frequencies were higher when the animals were moving up the thermal gradient ($\theta < 90$) than moving down the thermal gradient ($\theta > 90$) (Fig. 3*C*). We also measured the fraction of the exit direction Φ after the turns and the reversals, where Φ is the angle between the direction right after these behavioral events and the vector pointing to the warm side of the thermal gradient (Fig. 3*D*). In each event of turns and reversals, exit direction Φ was judged whether toward lower or higher temperature compared to the entry direction θ. We observed that among four types of reorientation behaviors (omega turn, shallow turn, reversal, reversal turn), the exit directions of shallow turns and reversals were biased toward the T_c in the $T < T_c$ and $T > T_c$ conditions; they were biased toward the higher temperature in the $T < T_c$ condition, whereas biased toward the lower temperature in the $T > T_c$ condition (Fig. 3*D*).

We also analyzed two components associated with forward movement: the curve direction and the locomotion speed. Curve direction was measured as the angle φ, the angle between the past and the current moving directions (Fig. 3*E* and Dataset S1). Similar to the exit directions of shallow turns and reversals, the curve direction was biased toward the warm side ($\varphi > 0$) in the $T < T_c$ condition and the cold side ($\varphi > 0$) in the $T > T_c$ condition (Fig. 3*E*). The locomotion speed also showed opposite biases under the $T < T_c$ or $T > T_c$ conditions. In the $T < T_c$ condition, the locomotion speed was faster when the animals were moving up the thermal gradient ($\theta < 90$) than moving down the thermal gradient ($\theta > 90$), whereas in the $T > T_c$ condition, the locomotion speed was faster when the animals were moving down the thermal gradient ($\theta > 90$) than moving up the thermal gradient ($\theta < 90$) (Fig. 3*F* and Dataset S1).

Under the $T >> T_c$ condition, the animals still maintained the biases in the frequencies of turns, but they no longer showed the regulation in the curve direction and the exit direction of turns and reversals (*SI Appendix*, Fig. S2 *C* and *D* and Dataset S1). These observations suggest that the loss of the regulation in these behavioral components might underlie the slower migration toward the T_c in the $T >> T_c$ condition.

We next assessed how the context-dependent behavioral regulations were influenced by the time course and the temperature experiences. The biases of turns, reversals, and curves in the $T > T_c$ condition were observed in the time windows earlier than the biases in the $T < T_c$ condition (*SI Appendix*, Fig. S3 *A–E* and Dataset S1), which may enable the faster migration toward the T_c when the animals are moving down toward the T_c than moving up toward the T_c (5, 11) (Fig. 1*C*). Interestingly, when the animals were assayed in one condition for 10 min and then repositioned in another condition (*SI Appendix*, Fig. S4*A*), thermotaxis in the new condition was influenced by the previous condition. When the new condition and the previous condition were similar (or different), animals showed faster (or slower) migration toward the T_c (*SI Appendix*, Fig. S4*B* and Dataset S1), and the biases in the behavioral components were observed in the earlier (or later) time windows (*SI Appendix*, Fig. S4 *C* and *D* and Dataset S1).

Taken together, our results suggest that depending on whether T is below or above the T_c, the behavioral components were oppositely biased, thereby enabling the animals to migrate toward the T_c.

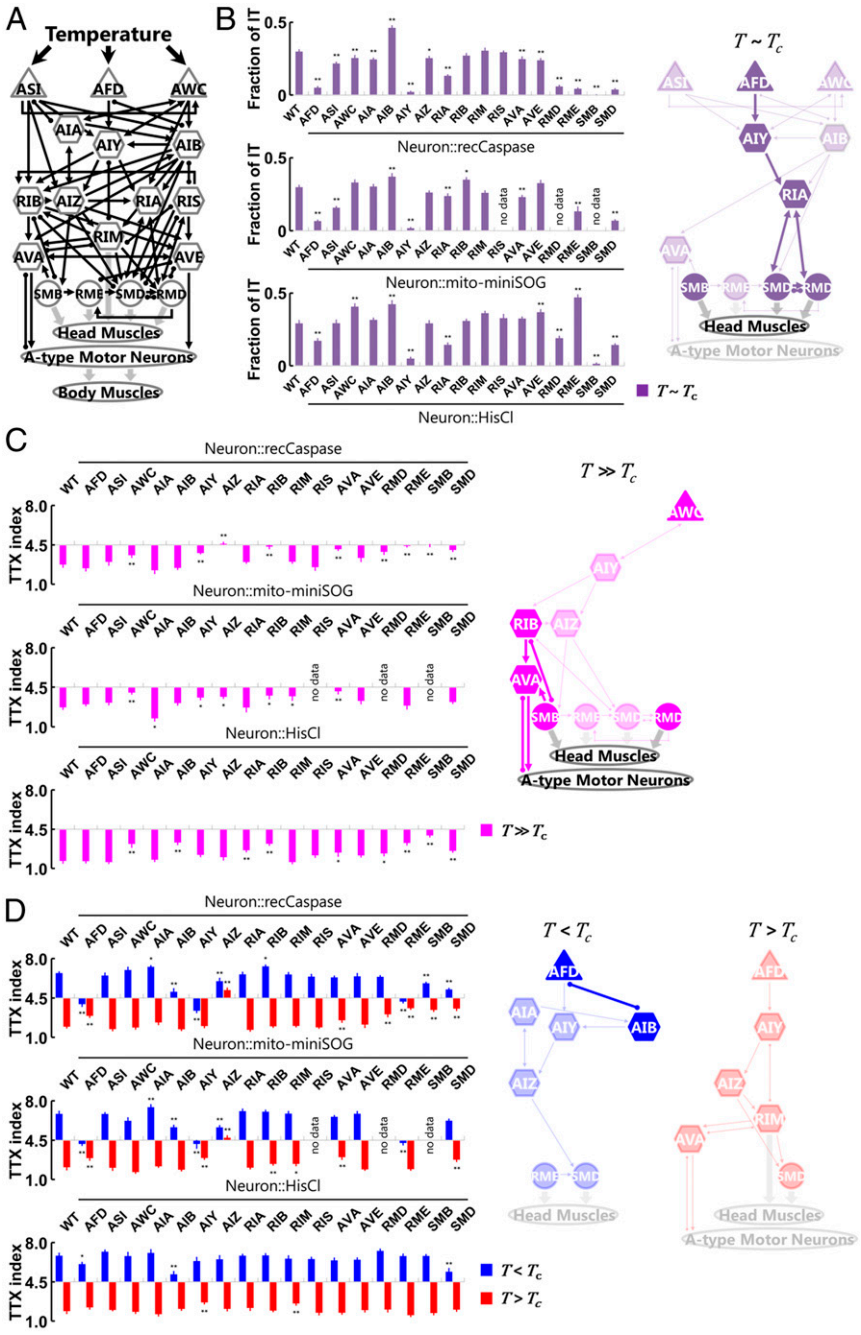

Fig. 2. Distinct sets of neurons are involved in the isothermal tracking (IT) and in the migration up or down toward the T_c. (*A*) Candidate neurons for cell-specific ablations, including thermosensory neurons (triangles), interneurons (hexagons), and head motor neurons (circles). Black thin arrows indicate chemical synapses, black undirected lines with round endings indicate gap junctions, and gray thick arrows indicate neuromuscular junctions. (*B*, *Left*) Fractions of IT during 30 to 60 min after the start of the assays ($n = 4$ to 12) of wild-type (WT) animals and the cell-ablated/silenced animals expressing reconstituted caspases (*Upper*), mito-miniSOG (*Middle*), or HisCl1 (*Lower*). *B*, *Right* is a neural diagram for mediating IT in the $T \sim T_c$ condition. The neurons in which their removal showed significant impairment of IT fraction in all of the genetic manipulations are shown in deep color, and the neurons in which their removal showed significant impairment or enhancement in at least two of three manipulations are shown in pale color. (*C* and *D*, *Left*) TTX indices at 60 min after the start of the assays ($n = 5$ to 12) of WT animals and the cell-ablated/silenced animals expressing reconstituted caspases (*Upper*), mito-miniSOG (*Middle*), or HisCl1 (*Lower*). The indices in the $T >> T_c$ condition are represented as magenta columns (*C*), the indices in the $T < T_c$ condition as blue columns, and the indices in the $T > T_c$ condition as red columns (*D*). *Right* are neural diagrams for mediating the migrations toward the T_c in the $T >> T_c$ condition (magenta), in the $T < T_c$ condition (blue), and in the $T > T_c$ condition (red). The neurons in which their removal showed significant impairment of TTX index in all of the genetic manipulations are shown in deep color, and the neurons in which their removal showed significant impairment or enhancement in at least two of three manipulations are shown in pale color. Error bars indicate SEM. $^{**}P < 0.01$ and $^{*}P < 0.05$, different from WT, using Dunnett's multiple comparisons test.

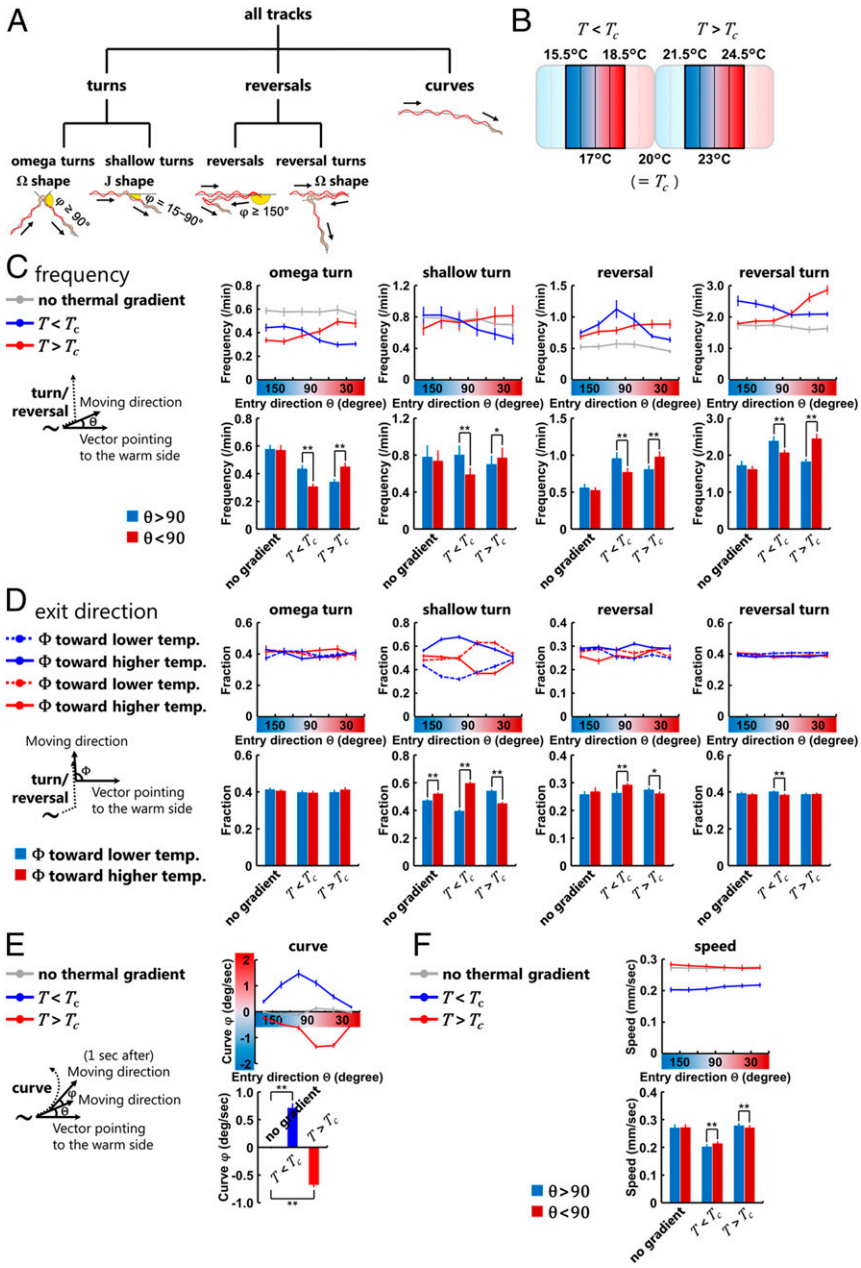

Fig. 3. Behavioral components are oppositely biased depending on the context. (*A*) Classification and definition of *C. elegans* behavioral components used in this study. Turns, reversals, and curves are classified as previously proposed (33–36). (*B*) Temperature range within which the behavioral components were analyzed. Animals in the center four fractions of the assay plate were analyzed. (*C*, *Upper Right*) Frequency plots of the turns and the reversals representing the average as a function of the entry direction θ (*Left*). (*C*, *Lower Right*) Comparisons of the frequency of each behavioral event. Deep blue columns indicate the frequencies while the animals are moving down the thermal gradient (θ > 90), and deep red columns indicate the frequencies while moving up the thermal gradient (θ < 90). (*D*) Fraction plots of the exit direction Φ after the turns and the reversals (*Left*) representing the average as a function of the entry direction θ (*Upper Right*) and the averages in all of the moving directions of animals (*Lower Right*). Dashed lines and deep blue columns indicate the fraction of Φ biased toward the lower temperature, and solid lines and deep red columns indicate the fraction of Φ biased toward the higher temperature. (*E*) Plots of the biases φ of curves (*Left*) representing the averages as a function of the entry direction θ (*Upper Right*) and the averages in all of the moving direction of animals (*Lower Right*). φ is defined as positive if biased toward higher temperature and negative if biased toward lower temperature. (*F*, *Upper*) Speed plots representing the averages as a function of the entry direction θ. Deep blue columns (*Lower*) indicate the speeds while the animals are moving down the thermal gradient (θ > 90), and deep red columns indicate the speeds while moving up the thermal gradient (θ < 90). In *C*–*F*, gray lines correspond to experiments without the thermal gradient (20 °C constant), blue lines correspond to experiments in the $T < T_c$ condition, and red lines correspond to experiments in the $T > T_c$ condition ($n = 9$ to 12). Error bars indicate SEM. (*C*, *D*, and *F*) $^{**}P < 0.01$ and $^{*}P < 0.05$ using paired Student's *t* test; (*E*) $^{**}P < 0.01$ using one-way ANOVA followed by a Tukey–Kramer post hoc multiple comparisons test.

Behavioral Components Differently Contribute to Thermotaxis Depending on Thermal Context. Although the biases of behavioral components (Fig. 3 *C*–*F*) likely play essential roles in thermotaxis, whether those biases are necessary and sufficient to migrate toward the T_c (Fig. 1*C*) is unclear. To address this question, we conducted Monte Carlo simulations of animals' migrations on the thermal gradient. In the simulation, we defined an animal's state by its position in the assay plate (x, y) and the direction of its movement relative to the vector pointing to the warm side of the thermal gradient (θ) (Fig. 4*A*). We updated the states of animals every second,

according to the experimental data of the turning frequencies, the exit directions of turns and curves (Φ and φ), and speeds (v), as functions of θ and T versus T_c (*SI Appendix*, Fig. S3 *A–F* and *Materials and Methods*). Similar to the animals observed in thermotaxis assays, computer-simulated animals (sims) moved up and down the thermal gradient toward the T_c within 30 min (Fig. 4*B*, Movie S2, and Dataset S3), suggesting that the biases in the behavioral components shown in Fig. 3 *C–F* are sufficient for the animals to reach the T_c.

We used this computational model of thermotaxis to examine the contributions of individual behavioral components. First, we simulated the situations in which sims could not use one of the behavioral components (*SI Appendix*, *Materials and Methods*). In the $T < T_c$ condition, the removal of the curves most severely impaired the increase of the TTX index. In the $T > T_c$ condition, the removal of the reversal turns showed the largest effect on the decrease of the TTX index (Fig. 4*C* and Dataset S3). Second, we performed the simulations in which sims used only one of the

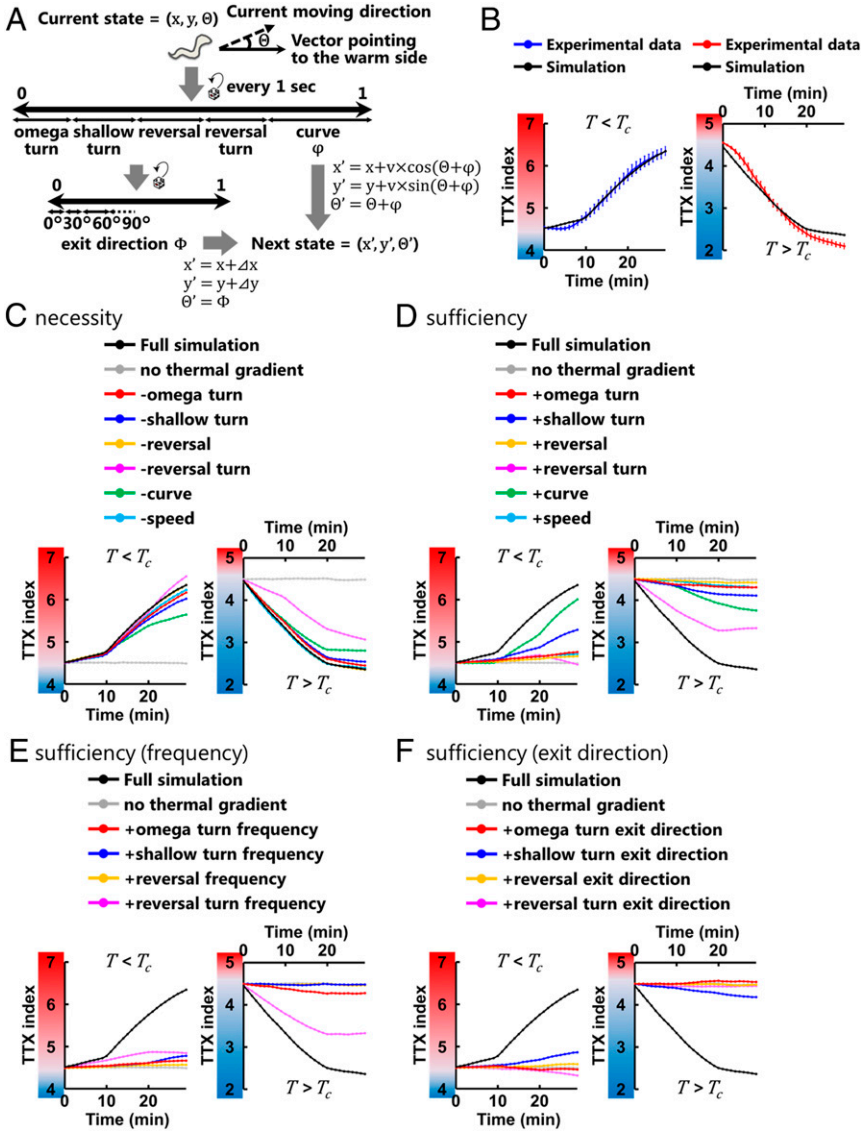

Fig. 4. Behavioral components are employed differently depending on the context. (*A*) Schematic structure of the thermotaxis behavior simulation. Animal's state was defined by its position (x, y) and moving direction relative to the vector pointing to the warm side (θ). We updated the states of the animal every second according to the experimentally observed data: the frequencies and the exit directions (Φ) of the turns and the reversals, the biases of the curves (φ), and the speeds (v), all of which were applied as functions of θ and T versus T_c. The displacements during the individual turns (Δx, Δy) were also employed when updating the states of the animals. (*B*) The time course of TTX indices in the simulations (black lines) and that obtained from experimental data (colored lines). In the simulations, we iterated assays 100 times, each with 100 animals, and the TTX indices were averaged within the assays. Error bars indicate SEM. (*C*) The time course of TTX indices in the simulations in which the data of the individual behavioral components determined by the experiment with the thermal gradient were replaced with the data of the corresponding component without the gradient. (*D–F*) The time course of TTX indices in the simulations in which the data of the individual behavioral components without the thermal gradient were replaced with the data of the corresponding components with the gradient. (*D*) Data of both frequencies and exit directions were replaced. (*E*) Data of frequencies alone were replaced. (*F*) Data of exit directions alone were replaced. In *C–F*, black lines correspond to the simulation in which all of the data of wild-type animals determined by the experiment with the thermal gradient were used, and gray lines correspond to the simulation in which all of the data of wild-type animals without the gradient were used. The other colored lines correspond to the simulation with the replacements of the individual behavioral components: the omega turn (red lines), the shallow turn (blue lines), the reversal (yellow lines), the reversal turn (magenta lines), the curve (green lines), and the speed (light blue lines).

behavioral components. In the $T < T_c$ condition, the sims using only the curves showed the most dramatic increase of the TTX index (Fig. 4*D* and Dataset S3), and the sims using only the shallow turns showed the second most dramatic increment of the index. In the $T > T_c$ condition, the reversal turns were most effective in decreasing the TTX index, and the curves were the second most effective.

The contribution of turns and reversals can be further dissected into the regulation of frequencies and exit directions, since both of these components showed biases during thermotaxis (Fig. 3 *C* and *D*). Therefore, we ran further simulations that only used one of these biases to assess how each contributes to the migration toward the T_c. Sims that used only the frequency of reversal turns showed significant changes in the TTX index toward T_c in the $T < T_c$ and $T > T_c$ conditions (Fig. 4*E* and Dataset S3), whereas the sims that used only the exit direction of reversal turns did not show any change in the TTX index (Fig. 4*F* and Dataset S3). By contrast, the sims that used only the exit direction of shallow turns showed a change in the index toward T_c in the $T < T_c$ and $T > T_c$ conditions (Fig. 4*F* and Dataset S3), whereas the sims that used only the frequency showed only a little increment in the $T < T_c$ condition (Fig. 4*E* and Dataset S3). These results suggest that the biases in the frequency of reversal turns contribute to the migration of the animals toward the T_c, whereas the biases in the exit direction of shallow turns contribute to the migration toward the T_c.

These results suggest that *C. elegans* use different behavioral strategies depending on thermal context: $T < T_c$ or $T > T_c$ conditions (Fig. 4 *C* and *D*). However, it is also possible that the absolute temperature may be solely responsible, since the animals are migrating in different temperature ranges in these experiments (Fig. 3*B*). Indeed, temperature itself is known to affect the turning frequencies and the speed of animals (12) (*SI Appendix*, Fig. S3*G*). To exclude the possibility that absolute temperature is solely responsible, we designed experiments that kept the temperature range constant and varied the cultivation temperature: the center of the assay plate was set at 20 °C and the T_c was set at 14 °C, 17 °C, 23 °C, or 25 °C (*SI Appendix*, Fig. S5 *A–C* and Dataset S1). We found that under these conditions, the animals displayed opposing biases in behavioral components (*SI Appendix*, Fig. S5 *D–G* and Dataset S1) similar to our aforementioned results when T_c was constant and the center temperature varied (Fig. 3 *C–F*). Also, the biases in the curves and the reversal turns differently contributed to the migration (*SI Appendix*, Fig. S5*H* and Dataset S3), suggesting that relative position to the T_c, but not absolute temperature, is important in controlling which behavioral strategies are employed. Taken together, our results show that the animals switch thermotactic behavioral strategies depending on the thermal context.

Distinct Sets of Neurons Are Responsible for Context-Dependent Regulation of Individual Behavioral Components. To identify neurons required for generating the biases in the behavioral components, we performed thermotaxis simulations using the experimental data of cell-ablated/silenced animals (*SI Appendix*, Fig. S6 and Datasets S4–S8). Sims were allowed to use only the data of the frequency (or exit direction) of each behavioral component from the wild-type or cell-ablated/silenced data. To assess the impact of a single-cell ablation/silencing on the regulation of each behavioral component, we calculated a migration index following the equation shown in Fig. 5*A*. This index is 0 when biases of the behavioral components of cell-ablated/silenced sims do not achieve any migration toward the T_c and 1 when biases achieve the same migration as wild-type sims.

Our analyses showed that for the regulation of even the same behavioral components, distinct sets of neurons are required under the $T < T_c$ or $T > T_c$ conditions (Fig. 5*B* and *SI Appendix*, Fig. S7*A*). For example, the single ablation/silencing of AIY and RIS impaired the migration indices of reversal turns in the $T < T_c$ condition, whereas the single ablations/silencing of AWC and AIA impaired the indices of reversal turns in the $T > T_c$ condition (Fig. 5*B*, *SI Appendix*, Fig. S6*A*, and Dataset S4). We applied the same analyses on the curves (Fig. 5*B*, *SI Appendix*, Fig. S6*B*, and Dataset S5), the exit directions of shallow turns (*SI Appendix*, Figs. S6*C* and S7*A* and Dataset S6), the frequencies of omega turns (*SI Appendix*, Figs. S6*D* and S7*A* and Dataset S7), and the speeds (*SI Appendix*, Figs. S6*E* and S7*A* and Dataset S8).

Similar to the reversal turns, several cell ablations and silencing showed different impact on the indices in the $T < T_c$ or $T > T_c$ conditions; the single ablation/silencing of AWC impaired the indices of the curves only in the $T < T_c$ condition, whereas the single ablation/silencing of AVA impaired the indices of the curves only in the $T > T_c$ condition. Likewise, the single ablation/silencing of AIY impaired the indices of the shallow turns in the $T < T_c$ condition but did not significantly influence the indices of the shallow turns in the $T > T_c$ condition, and the single ablation/silencing of AIZ lowered the indices of the speeds in the $T > T_c$ condition but not in the $T < T_c$ condition. These context-dependent requirements of distinct sets of neurons were also predicted by comparing another index (32) (*SI Appendix*, Fig. S8), which calculates biases in the behavioral components directly from the observed profiles (see legend of *SI Appendix*, Fig. S8).

Our study also found that some single-cell ablation and silencing enhanced the biases in behavioral components (*SI Appendix*, Figs. S6 and S8), thereby resulting in the enhanced increase or decrease in the simulation analyses (Fig. 5 *C* and *D* and *SI Appendix*, Fig. S7 *B–D*). These unexpected enhancements potentially lead to the normal migration toward the T_c of cell-ablated/silenced animals (Fig. 2*D* and *SI Appendix*, Fig. S1*B*).

In addition to the neurons required for generating the biases in the behavioral components (Fig. 5 and *SI Appendix*, Figs. S7 and S8), we were able to identify sets of neurons that regulate the basal level of turns, reversals, and speeds (*SI Appendix*, Fig. S9). We found that the involvement of these neurons was relatively independent of the thermal context; 80% of the neurons listed in *SI Appendix*, Fig. S9 were involved in the regulation of the basal level of the behavioral components in both $T < T_c$ and $T > T_c$ conditions, whereas 41% of the neurons listed in *SI Appendix*, Fig. S8 participated in the bias in the behavioral components in both conditions. Taken together, our results show that depending on the thermal context, distinct sets of neurons are required to generate the biases in the individual behavioral components.

Thermal Context Is Evaluated in Two Sensory Neurons and Evokes Bidirectional Responses in an Interneuron. To understand how context-dependent information processing is implemented in the identified sets of neurons, we monitored the neural activities of representative sensory neurons AFD and AWC, and a first-layer amphid interneuron AIB (Fig. 6*A*). These neurons are involved in the regulation of the reversal turns and the curves under the $T < T_c$ and/or $T > T_c$ conditions (Fig. 5*B*). We performed calcium imaging in freely moving animals using the single-worm tracking system (37) (Fig. 6*B*). Correlation analysis of the temperature input versus the standardized YFP/CFP fluorescence ratio change from baseline (*SI Appendix*, *Materials and Methods*) revealed that the Ca^{2+} signal of the AFD sensory neuron versus the absolute temperature showed stronger correlation in the $T > T_c$ than $T < T_c$ conditions (Fig. 6*C*), whereas the Ca^{2+} signal of AFD versus the differential of temperature showed stronger correlation in the $T < T_c$ than $T > T_c$ condition (Fig. 6*C*). By contrast, the Ca^{2+} signal of AWC sensory neuron versus the absolute temperature only showed a strong correlation in the $T > T_c$ condition (Fig. 6 *B* and *C*). These observations suggest that sensory neurons AFD and AWC implement the context-dependent encoding of thermal signals. Interestingly, the activity of the AIB interneuron showed opposite correlations with

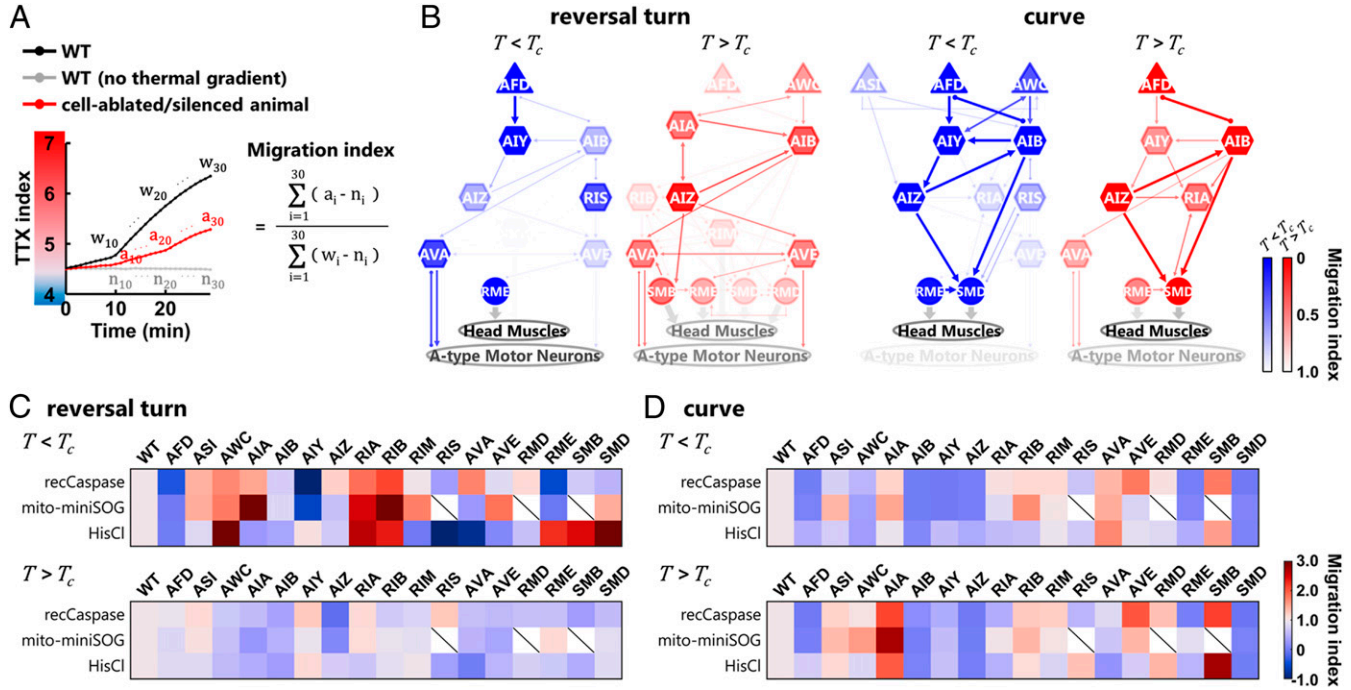

Fig. 5. Distinct sets of neurons are responsible for the context-dependent biases in the behavioral components. (*A*) Formula for the migration index. TTX indices from the simulation of cell-ablated animals (a_i, red line) were compared with the indices from the simulation of WT animals without the thermal gradient (n_i, gray line) in every minute, and the difference between them was summed up within 1 to 30 min. The value was normalized with the summation of the difference between the TTX indices from the simulation of WT with the thermal gradient (w_i, black line) and the indices of WT without the gradient. (*B*) Neural diagrams responsible for generating the biases in the reversal turns and the curves in the $T < T_c$ condition (blue) and in the $T > T_c$ condition (red). The thickness and color strength of each neuron represent the functional importance of the neuron predicted from the analysis and were determined as follows: For each neuron, the differences between the migration index of the wild-type animals and the index of the cell-ablated/silenced animals expressing reconstituted caspases, mito-miniSOG, or HisCl1 were calculated. The median difference from the three ablation strategies (or the smaller difference from the two strategies) is used to determine the color strength, where the color strength of each neuron is proportional to this value. The color strength of each line is identical to the strength of the color of one of the two connected neurons with lower strength, and the thickness of each line is proportional to this color strength. (*C* and *D*) Heatmaps showing migration indices of the reversal turns (*C*) and the curves (*D*) after cell-specific ablation and silencing in the $T < T_c$ condition (*Upper*) and in the $T > T_c$ condition (*Lower*).

both absolute temperature and the differential temperature under the $T < T_c$ and $T > T_c$ conditions (Fig. 6*C*).

We next monitored the neural activities in immobilized animals. Consistent with the freely moving conditions, the standardized GCaMP fluorescence ratio change of AIB decreased upon warming and increased upon cooling in the $T < T_c$ condition, whereas the Ca^{2+} signal increased upon warming and decreased upon cooling in the $T > T_c$ condition (Fig. 6*D* and Dataset S9). We further monitored the Ca^{2+} signal of AIB in AFD-ablated animals and AWC-ablated animals. In the $T < T_c$ condition, the decrement of the Ca^{2+} signal upon warming was weakened by the ablation of AFD (Fig. 6*E* and Dataset S9). By contrast, in the $T > T_c$ condition, the increment of the Ca^{2+} signal upon warming was diminished by the ablation of AFD or AWC.

These results suggest that thermal signals sensed by AFD and AWC evoke bidirectional responses in AIB under the $T < T_c$ or $T > T_c$ conditions, which potentially leads to the thermal context-dependent operation in distinct downstream interneurons (Fig. 6*A*) and opposing regulation of the reversal turns and the curves.

Discussion

In this study, we show that context-dependent navigation of *C. elegans* on thermal gradients is mediated by opposing biases in individual behavioral components and that distinct sets of neurons are required for the opposing regulation of even the same behavioral components (Fig. 5 and *SI Appendix*, Fig. S7). Our imaging analyses suggested that context-dependent behavioral regulation originates early in the neural pathways with sensory and first-layer interneurons responding differently to the same type of thermal inputs (Fig. 6), thereby potentially leading to context-dependent operation of downstream neural circuits.

Given such context-dependent aspects in the nervous system, future investigation of neural circuits and behavioral regulation should be performed under appropriate discrimination of environmental contexts. For instance, we found that depending on whether the animals were moving below or above the T_c, distinct behavioral components, curves or reversal turns, were employed to migrate to the T_c (Figs. 3 and 4). In the region far above T_c, the animals could not employ curves and shallow turns to migrate toward the T_c (*SI Appendix*, Fig. S4). Such context-dependent behavioral regulation is also observed upon switching between escape and avoidance from noxious heat (35) and switching between reversal and curve during acidic pH avoidance (38). Even during a continuous navigation behavior, distinct behavioral strategies are executed depending on the distance from a destination, each of which is performed via distinct sensory neurons (39). These observations tell us that the discrimination of environmental contexts is a critical step to investigate the nervous system.

Comprehensive cell ablation and silencing experiments (Fig. 2*A*) showed that many of the cell-ablated/silenced animals could migrate toward the T_c (Fig. 2*D* and *SI Appendix*, Fig. S1*B*). Such robust migration of animals with deficient neural circuits was observed in previous studies (11, 15) and have complicated identification of neural circuits for thermotaxis behavior. One plausible explanation for this observation could be redundancy in the nervous system. Redundancy among neurons is well known (15, 40) and might explain the scatter of the neurons in the

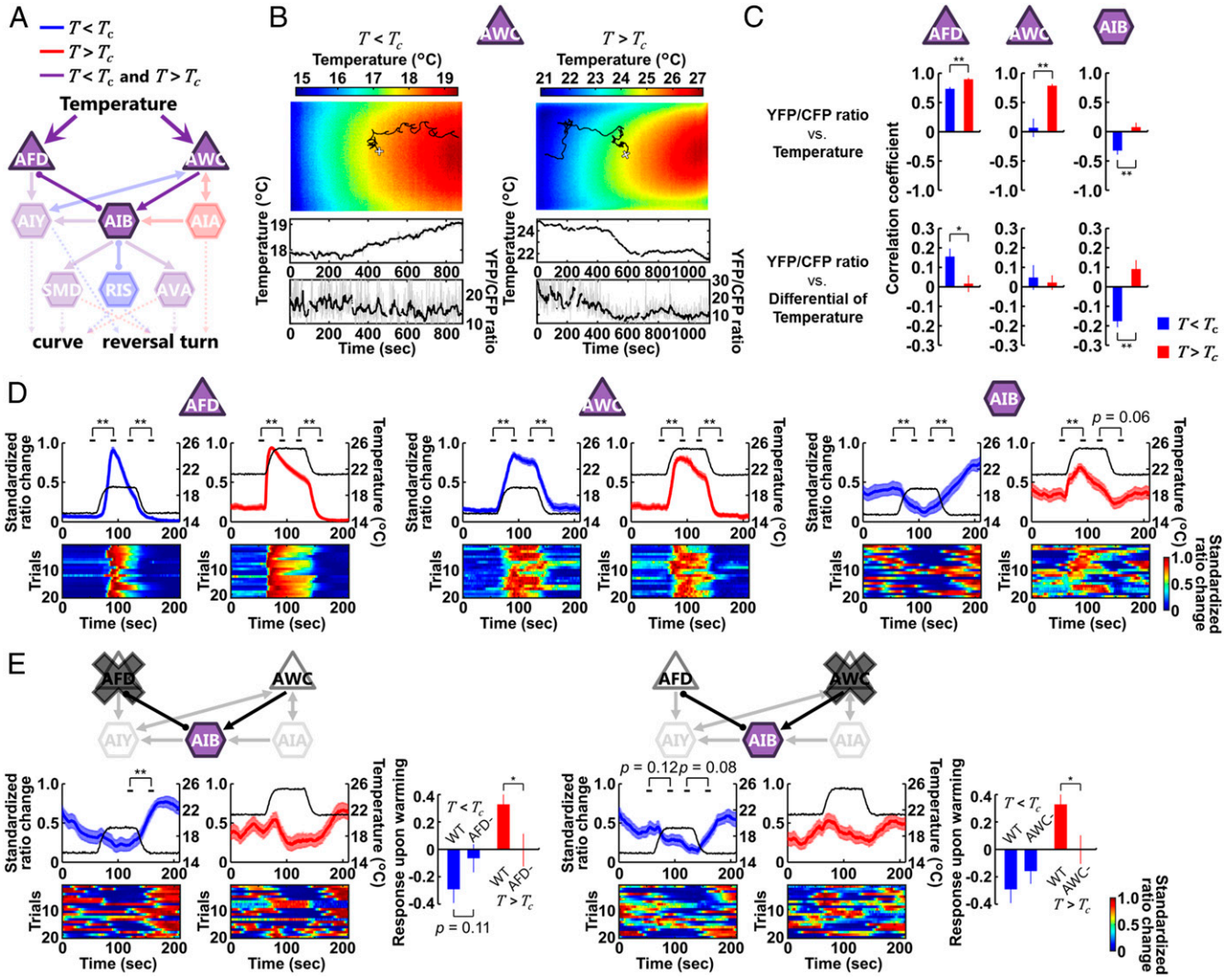

Fig. 6. Difference of the context is encoded in AFD and AWC thermosensory neurons and evokes opposing responses in AIB. (*A*) Representative sensory neurons and first-layer interneurons that regulate the curves or the reversal turns in the $T < T_c$ condition (blue), in the $T > T_c$ condition (red), or in both conditions (purple). Thin arrows indicate chemical synapses and an undirected line with round endings indicates gap junction. (*B*, *Upper*) Representative trajectory of an animal (black line) projected on a thermography image, providing the time course of the temperature changes (*Middle*). The white + marks the starting point when recording starts. The YFP/CFP ratio was calculated from YFP and CFP fluorescences of the fluorescence resonance energy transfer (FRET)-based calcium probe yellow cameleon × 1.60 expressed in the individual neurons (*Lower*). The gray line denotes the ratio, and the black line denotes the median for the time series of the ratio (*SI Appendix, Materials and Methods*). (*C*) Calcium imaging of AFD, AWC, and AIB in freely moving animals. Correlation analysis of the standardized ratio change of the individual neurons versus the absolute temperature (*Upper*) and the differential of temperature (*Lower*) in the $T < T_c$ condition (blue columns) and in the $T > T_c$ condition (red columns) was performed ($n = 14$ to 17). (*D* and *E*) Calcium imaging of AFD, AWC, and AIB in immobilized animals. (*Upper*) Standardized ratio changes of the individual neurons ($n = 20$ to 21). Two types of temperature stimuli (black lines) were used: 15 to 19 to 15 °C and 21 to 25 to 21 °C linear warming and cooling. Average standardized ratio changes for 10 s before and after temperature transitions were compared. The differences between average standardized ratio changes of AIB for 10 s after and before temperature increment were defined as responses upon warming. (*Lower*) Heatmaps of standardized ratio changes (blue = 0, red = 1.0). Error bars and shaded regions around traces indicate SEM. (*C* and *E*) $^{**}P < 0.01$ and $^{*}P < 0.05$ using Student's *t* test. (*D* and *E*) $^{**}P < 0.01$ and $^{*}P < 0.05$ using paired Student's *t* test.

neural diagrams (Fig. 2 *C* and *D*). In addition to redundancy, our analysis of behavioral components (Fig. 3*A*) combined with modeling analysis (Fig. 4*A*) suggests two mechanisms that could underlie robust execution of behavior: compensation and antagonistic effects of behavioral components. We found that in certain cell-ablated animals, biases in some behavioral components were impaired, while biases in other components were significantly enhanced. For example, in RIS-ablated animals, the bias in the curves and the shallow turns was markedly reduced in the $T < T_c$ condition, while the bias in the reversal turns was strengthened (Fig. 5 *C* and *D* and *SI Appendix*, Fig. S7*B*), thereby compensating the impairments in the curves and the shallow turns and generating normal migrations. Another potential mechanism might be due to the lack of antagonistic effect of reorientation behavior on migration: for example, AIB-ablated animals displayed low basal frequency of reversal turns (*SI Appendix*, Fig. S9). We speculated that such low frequency of reversal turns weakens the antagonistic effect of reversal turns on migration, allowing the animals to travel a long distance toward the right direction with marginal biases in other behavioral components. These compensatory and antagonistic relationships among behavioral components could explain some of the unexpected normal migrations shown in Fig. 2*D* and *SI Appendix*, Fig. S1*B*. Overall, it would be important to take these principles into consideration when

studying other types of behavior, such as chemotaxis (32, 41, 42) or exploratory behavior (43), also in other model animals. In crustacean and mammalian brain networks, robustness is an obstacle for inferring functional connections that can only be resolved by applying statistical methods (44, 45). Our observations suggest that by subdividing behavior into components, we can assess the contribution of individual neurons and link the nervous system with the behavior.

Extending the above ideas, appropriate subdivisions of behavior might provide better opportunity to identify relevant neural circuits for behavioral regulations. In our study, the neural diagram for reversal turns and curves are relatively well defined (Fig. 5*B* and *SI Appendix*, Fig. S6 *A* and *B*), suggesting that these subdivisions were successful. By contrast, the diagrams for shallow turns and omega turns were less defined, in which most of the neurons exhibit subtle contributions (*SI Appendix*, Figs. S6 *C* and *D* and S7*A*), suggesting that other classifications of turns might be needed to fully elucidate their underlying circuitry, as some possible classifications have been previously proposed (34, 46). Also, nonrule-based classifications of behaviors (47, 48), especially the description of the state of the animal in shape space (49), are reported to be successful in assessing the impact of cell ablations (50, 51) and might enable the definition of further defined neural diagrams.

We observed that a first-layer interneuron, AIB, shows bidirectional responses to the same kind of thermal inputs under the $T < T_c$ or $T > T_c$ conditions in freely moving animals (Fig. 6*C*). Also in immobilized animals, temperature increment inhibits AIB and decrement excites AIB in the $T < T_c$ condition, whereas temperature increment excites AIB and decrement inhibits AIB in the $T > T_c$ condition (Fig. 6*D*). Since the activity of AIB is positively correlated with the execution of reversal turning (41, 52), the context-dependent response of AIB would generate opposing biases in the reversal turns; the frequency of reversal turns becomes lower when animals are moving toward the T_c, whereas the frequency becomes higher when moving away from the T_c (Fig. 3*C*). The neural diagram in Fig. 5*B* shows the possibility that the responses of AIB are transmitted to motor neurons via RIS, AVA, or RIM as proposed in previous studies (53, 54). Also, the context-dependent response of AIB could generate opposing biases in the curves and the shallow turns, considering previous studies show that activation and inhibition of an interneuron can uniformly enhance or reduce curving angle (24, 55).

Since AFD and AIB are connected by gap junctions (56) and AWC transmits excitatory signals to AIB (57), it makes sense that thermal signals from AFD and AWC both show positive correlation with AIB activity in the $T > T_c$ condition (Fig. 6 *C* and *D*). Both the ablations of AFD and AWC indeed abolished the increment of AIB activity upon warming in the $T > T_c$ condition (Fig. 6*E*). By contrast, it is not obvious how negative correlation between thermal signals and AIB activity in the $T < T_c$ condition is generated. We observed that the ablation of AFD weakened the decrement of AIB activity upon warming in the $T < T_c$ condition (Fig. 6*E*); thus AFD might also transmit inhibitory signals to AIB. One candidate mechanism of such a context-dependent signaling is the transmission of neuropeptides from AFD (58–60). A growing body of evidence suggests that neuropeptide signaling modulates synaptic activities depending on external and internal contexts (42, 61, 62). Such alterations in synaptic valence can drive distinct neural and behavioral responses to identical stimuli, thus potentially underlying the context-dependent behavioral regulations in this study. Cooperative interaction with other sensory neurons, including AWC, might also generate context-dependent responses of AIB. A recent study shows that AIB oppositely responds to increasing or decreasing of gustatory stimulus via inhibitory signal from the ASEL sensory neuron and/or excitatory signal from the ASER sensory neuron (63). Both signals are glutamatergic, but are received by distinct types of glutamate receptor located in AIB, evoking opposing responses. Another candidate mechanism for the context-dependent response of AIB is feedback from downstream neurons. In interneuron and motor neuron layers, the motor command sequences are always represented even when the animals are not moving (23, 52, 64). Therefore, the activities of the upstream interneurons could be modulated by those pervasive dynamics. Indeed, the response of AIB to odor stimuli via the AWC sensory neuron is affected by the state of the downstream interneurons RIM and AVA (54). Some studies have suggested that sensory inputs could be converted into appropriate motor outputs after being integrated with those dynamics (65, 66). Also in mammalian brains, feedback from downstream neurons is known to play an important role in the visual (67) and somatosensory systems (68). These interactions with pervasive dynamics might result in the context-dependent operation of neural circuits (Fig. 5*B* and *SI Appendix*, Fig. S7), which may be a prevalent strategy for the nervous system to execute flexible behavioral regulation.

Materials and Methods

Thermotaxis assays, behavioral recording, and calcium imaging were performed as previously described (5, 16, 37, 48). For detailed information on all methods, see *SI Appendix, Materials and Methods*.

Data Availability. All data and associated protocols used for this study are available in the main manuscript and *SI Appendix*. Source code is available at GitHub, https://github.com/ikedamuneki/ThermotaxisAnalysis. Materials used for this study will be available upon requests to the corresponding author.

ACKNOWLEDGMENTS. We thank Martin Chalfie for the reconstituted caspases construct (Addgene plasmids 16082 and 16083); Yishi Jin for the mito-miniSOG construct; Seika Takayanagi-Kiya for advice on the usage of mito-miniSOG; Cornelia Bargmann for the HisCl1 strain, the construct, and the protocol; Erik Jorgensen for the flippase and flippase recognition target construct; Piali Sengupta for the ASI-ablated strain; Shin Takagi for the unpublished AVE marker strain; Kaveh Ashrafi for the *mgl-1* promoter; Mario de Bono for the *npr-4a* promoter; Shawn Xu for information about the *sto-3* promoter; and Eduardo Izquierdo for advice on the assessment of the simulation. M.I. was supported by Grant-in-Aid for Scientific Research (KAKENHI) 16J05770, A.C.G. was supported by Japan Society for the Promotion of Science Postdoctoral Fellowship PE12065, and this work was supported by KAKENHI 18H05123 (to S.N.) and 16H02516, 16H01272, 18H04693, 19H01009, and 19H05644 (to I.M.).

1. F. S. Gottfried, G. L. Donald, *The Orientation of Animals: Kineses, Taxes and Compass Reactions* (Dover Publications, 1961).
2. H. Dingle, V. A. Drake, What is migration? *Bioscience* **57**, 113–121 (2007).
3. T. J. Stevenson, V. Kumar, Neural control of daily and seasonal timing of songbird migration. *J. Comp. Physiol. A Neuroethol. Sens. Neural Behav. Physiol.* **203**, 399–409 (2017).
4. R. Wehner, B. Michel, P. Antonsen, Visual navigation in insects: Coupling of egocentric and geocentric information. *J. Exp. Biol.* **199**, 129–140 (1996).
5. H. Ito, H. Inada, I. Mori, Quantitative analysis of thermotaxis in the nematode *Caenorhabditis elegans*. *J. Neurosci. Methods* **154**, 45–52 (2006).
6. E. M. Hedgecock, R. L. Russell, Normal and mutant thermotaxis in the nematode *Caenorhabditis elegans*. *Proc. Natl. Acad. Sci. U.S.A.* **72**, 4061–4065 (1975).
7. P. Jurado, E. Kodama, Y. Tanizawa, I. Mori, Distinct thermal migration behaviors in response to different thermal gradients in *Caenorhabditis elegans*. *Genes Brain Behav.* **9**, 120–127 (2010).
8. D. Ramot, B. L. MacInnis, H.-C. Lee, M. B. Goodman, Thermotaxis is a robust mechanism for thermoregulation in *Caenorhabditis elegans* nematodes. *J. Neurosci.* **28**, 12546–12557 (2008).
9. I. Mori, Y. Ohshima, Neural regulation of thermotaxis in *Caenorhabditis elegans*. *Nature* **376**, 344–348 (1995).
10. N. A. Croll, Components and patterns in the behaviour of the nematode *Caenorhabditis elegans*. *J. Zool.* **176**, 159–176 (1975).
11. L. Luo *et al.*, Bidirectional thermotaxis in *Caenorhabditis elegans* is mediated by distinct sensorimotor strategies driven by the AFD thermosensory neurons. *Proc. Natl. Acad. Sci. U.S.A.* **111**, 2776–2781 (2014).
12. W. S. Ryu, A. D. T. Samuel, Thermotaxis in *Caenorhabditis elegans* analyzed by measuring responses to defined Thermal stimuli. *J. Neurosci.* **22**, 5727–5733 (2002).
13. A. Kuhara *et al.*, Temperature sensing by an olfactory neuron in a circuit controlling behavior of *C. elegans*. *Science* **320**, 803–807 (2008).

14. D. Biron, S. Wasserman, J. H. Thomas, A. D. T. Samuel, P. Sengupta, An olfactory neuron responds stochastically to temperature and modulates *Caenorhabditis elegans* thermotactic behavior. *Proc. Natl. Acad. Sci. U.S.A.* **105**, 11002–11007 (2008).
15. M. Beverly, S. Anbil, P. Sengupta, Degeneracy and neuromodulation among thermosensory neurons contribute to robust thermosensory behaviors in *Caenorhabditis elegans*. *J. Neurosci.* **31**, 11718–11727 (2011).
16. K. D. Kimura, A. Miyawaki, K. Matsumoto, I. Mori, The *C. elegans* thermosensory neuron AFD responds to warming. *Curr. Biol.* **14**, 1291–1295 (2004).
17. N. A. Swierczek, A. C. Giles, C. H. Rankin, R. A. Kerr, High-throughput behavioral analysis in *C. elegans*. *Nat. Methods* **8**, 592–598 (2011).
18. M. Ikeda, S. Nakano, A. C. Giles, L. Xu, I. Mori, Toolbox for analysis and simulation of *C. elegans* thermotaxis. GitHub. https://github.com/ikedamuneki/ThermotaxisAnalysis. Deposited 14 January 2020.
19. L. Luo, D. A. Clark, D. Biron, L. Mahadevan, A. D. T. Samuel, Sensorimotor control during isothermal tracking in *Caenorhabditis elegans*. *J. Exp. Biol.* **209**, 4652–4662 (2006).
20. M. Chalfie *et al*., The neural circuit for touch sensitivity in *Caenorhabditis elegans*. *J. Neurosci.* **5**, 956–964 (1985).
21. W. M. Roberts *et al*., A stochastic neuronal model predicts random search behaviors at multiple spatial scales in *C. elegans*. *eLife* **5**, e12572 (2016).
22. A. C. Hart, S. Sims, J. M. Kaplan, Synaptic code for sensory modalities revealed by *C. elegans* GLR-1 glutamate receptor. *Nature* **378**, 82–85 (1995).
23. M. Hendricks, H. Ha, N. Maffey, Y. Zhang, Compartmentalized calcium dynamics in a *C. elegans* interneuron encode head movement. *Nature* **487**, 99–103 (2012).
24. A. Kocabas, C.-H. Shen, Z. V. Guo, S. Ramanathan, Controlling interneuron activity in *Caenorhabditis elegans* to evoke chemotactic behaviour. *Nature* **490**, 273–277 (2012).
25. X. Ma, Y. Shen, Structural basis for degeneracy among thermosensory neurons in *Caenorhabditis elegans*. *J. Neurosci.* **32**, 1–3 (2012).
26. J. L. Donnelly *et al*., Monoaminergic orchestration of motor programs in a complex *C. elegans* behavior. *PLoS Biol.* **11**, e1001529 (2013).
27. Z. Li, J. Liu, M. Zheng, X. Z. S. Xu, Encoding of both analog- and digital-like behavioral outputs by one *C. elegans* interneuron. *Cell* **159**, 751–765 (2014).
28. I. Kotera *et al*., Pan-neuronal screening in *Caenorhabditis elegans* reveals asymmetric dynamics of AWC neurons is critical for thermal avoidance behavior. *eLife* **5**, e19021 (2016).
29. D. S. Chelur, M. Chalfie, Targeted cell killing by reconstituted caspases. *Proc. Natl. Acad. Sci. U.S.A.* **104**, 2283–2288 (2007).
30. Y. B. Qi, E. J. Garren, X. Shu, R. Y. Tsien, Y. Jin, Photo-inducible cell ablation in *Caenorhabditis elegans* using the genetically encoded singlet oxygen generating protein miniSOG. *Proc. Natl. Acad. Sci. U.S.A.* **109**, 7499–7504 (2012).
31. N. Pokala, Q. Liu, A. Gordus, C. I. Bargmann, Inducible and titratable silencing of *Caenorhabditis elegans* neurons in vivo with histamine-gated chloride channels. *Proc. Natl. Acad. Sci. U.S.A.* **111**, 2770–2775 (2014).
32. Y. Iino, K. Yoshida, Parallel use of two behavioral mechanisms for chemotaxis in *Caenorhabditis elegans*. *J. Neurosci.* **29**, 5370–5380 (2009).
33. J. T. Pierce-Shimomura, T. M. Morse, S. R. Lockery, The fundamental role of pirouettes in *Caenorhabditis elegans* chemotaxis. *J. Neurosci.* **19**, 9557–9569 (1999).
34. D. Kim, S. Park, L. Mahadevan, J. H. Shin, The shallow turn of a worm. *J. Exp. Biol.* **214**, 1554–1559 (2011).
35. L. C. Schild, D. A. Glauser, Dynamic switching between escape and avoidance regimes reduces *Caenorhabditis elegans* exposure to noxious heat. *Nat. Commun.* **4**, 2198 (2013).
36. L. C. M. Salvador, F. Bartumeus, S. A. Levin, W. S. Ryu, Mechanistic analysis of the search behaviour of *Caenorhabditis elegans*. *J. R. Soc. Interface* **11**, 20131092 (2014).
37. Y. Tsukada *et al*., Reconstruction of spatial thermal gradient encoded in thermosensory neuron AFD in *Caenorhabditis elegans*. *J. Neurosci.* **36**, 2571–2581 (2016).
38. T. Wakabayashi *et al*., Navigational choice between reversal and curve during acidic pH avoidance behavior in *Caenorhabditis elegans*. *BMC Neurosci.* **16**, 79 (2015).
39. E. Itskovits, R. Ruach, A. Zaslaver, Concerted pulsatile and graded neural dynamics enables efficient chemotaxis in *C. elegans*. *Nat. Commun.* **9**, 2866 (2018).
40. C. I. Bargmann, H. R. Horvitz, Chemosensory neurons with overlapping functions direct chemotaxis to multiple chemicals in C. elegans. *Neuron* **7**, 729–742 (1991).
41. L. Luo *et al*., Dynamic encoding of perception, memory, and movement in a *C. elegans* chemotaxis circuit. *Neuron* **82**, 1115–1128 (2014).
42. M. L. Guillermin, M. A. Carrillo, E. A. Hallem, A single set of interneurons drives opposite behaviors in *C. elegans*. *Curr. Biol.* **27**, 2630–2639.e6 (2017).
43. J. M. Gray, J. J. Hill, C. I. Bargmann, A circuit for navigation in *Caenorhabditis elegans*. *Proc. Natl. Acad. Sci. U.S.A.* **102**, 3184–3191 (2005).
44. S. Srinivasan, C. F. Stevens, Robustness and fault tolerance make brains harder to study. *BMC Biol.* **9**, 46 (2011).
45. D. J. Schwab, R. F. Bruinsma, J. L. Feldman, A. J. Levine, Rhythmogenic neuronal networks, emergent leaders, and k-cores. *Phys. Rev. E Stat. Nonlin. Soft Matter Phys.* **82**, 051911 (2010).
46. O. D. Broekmans, J. B. Rodgers, W. S. Ryu, G. J. Stephens, Resolving coiled shapes reveals new reorientation behaviors in *C. elegans*. *eLife* **5**, e17227 (2016).
47. A. E. X. Brown, E. I. Yemini, L. J. Grundy, T. Jucikas, W. R. Schafer, A dictionary of behavioral motifs reveals clusters of genes affecting *Caenorhabditis elegans* locomotion. *Proc. Natl. Acad. Sci. U.S.A.* **110**, 791–796 (2013).
48. S. Yamaguchi *et al*., Identification of animal behavioral strategies by inverse reinforcement learning. *PLOS Comput. Biol.* **14**, e1006122 (2018).
49. G. J. Stephens, B. Johnson-Kerner, W. Bialek, W. S. Ryu, Dimensionality and dynamics in the behavior of *C. elegans*. *PLOS Comput. Biol.* **4**, e1000028 (2008).
50. G. Yan *et al*., Network control principles predict neuron function in the *Caenorhabditis elegans* connectome. *Nature* **550**, 519–523 (2017).
51. I. Hums *et al*., Regulation of two motor patterns enables the gradual adjustment of locomotion strategy in *Caenorhabditis elegans*. *eLife* **5**, e14116 (2016).
52. S. Kato *et al*., Global brain dynamics embed the motor command sequence of *Caenorhabditis elegans*. *Cell* **163**, 656–669 (2015).
53. B. J. Piggott, J. Liu, Z. Feng, S. A. Wescott, X. Z. S. Xu, The neural circuits and synaptic mechanisms underlying motor initiation in *C. elegans*. *Cell* **147**, 922–933 (2011).
54. A. Gordus, N. Pokala, S. Levy, S. W. Flavell, C. I. Bargmann, Feedback from network states generates variability in a probabilistic olfactory circuit. *Cell* **161**, 215–227 (2015).
55. Y. Satoh *et al*., Regulation of experience-dependent bidirectional chemotaxis by a neural circuit switch in *Caenorhabditis elegans*. *J. Neurosci.* **34**, 15631–15637 (2014).
56. J. G. White, E. Southgate, J. N. Thomson, S. Brenner, The structure of the nervous system of the nematode *Caenorhabditis elegans*. *Philos. Trans. R. Soc. Lond. B Biol. Sci.* **314**, 1–340 (1986).
57. S. H. Chalasani *et al*., Dissecting a circuit for olfactory behaviour in *Caenorhabditis elegans*. *Nature* **450**, 63–70 (2007).
58. A. Narayan, G. Laurent, P. W. Sternberg, Transfer characteristics of a thermosensory synapse in *Caenorhabditis elegans*. *Proc. Natl. Acad. Sci. U.S.A.* **108**, 9667–9672 (2011).
59. A. N. Nathoo, R. A. Moeller, B. A. Westlund, A. C. Hart, Identification of neuropeptide-like protein gene families in *Caenorhabditis elegans* and other species. *Proc. Natl. Acad. Sci. U.S.A.* **98**, 14000–14005 (2001).
60. K. Kim, C. Li, Expression and regulation of an FMRFamide-related neuropeptide gene family in *Caenorhabditis elegans*. *J. Comp. Neurol.* **475**, 540–550 (2004).
61. S. G. Leinwand, S. H. Chalasani, Neuropeptide signaling remodels chemosensory circuit composition in *Caenorhabditis elegans*. *Nat. Neurosci.* **16**, 1461–1467 (2013).
62. S. H. Chalasani *et al*., Neuropeptide feedback modifies odor-evoked dynamics in *Caenorhabditis elegans* olfactory neurons. *Nat. Neurosci.* **13**, 615–621 (2010).
63. M. Kuramochi, M. Doi, An excitatory/inhibitory switch from asymmetric sensory neurons defines postsynaptic tuning for a rapid response to NaCl in *Caenorhabditis elegans*. *Front. Mol. Neurosci.* **11**, 484 (2019).
64. Q. Wen *et al*., Proprioceptive coupling within motor neurons drives *C. elegans* forward locomotion. *Neuron* **76**, 750–761 (2012).
65. H. Liu *et al*., Cholinergic sensorimotor integration regulates olfactory steering. *Neuron* **97**, 390–405.e3 (2018).
66. M. Hendricks, Y. Zhang, Complex RIA calcium dynamics and its function in navigational behavior. *Worm* **2**, e25546 (2013).
67. A. Pascual-Leone, V. Walsh, Fast backprojections from the motion to the primary visual area necessary for visual awareness. *Science* **292**, 510–512 (2001).
68. S. Manita *et al*., A top-down cortical circuit for accurate sensory perception. *Neuron* **86**, 1304–1316 (2015).